Available online at www.sciencedirect.com
SCIENCE DIRECT
ELSEVIER
International Journal of Mass Spectrometry 253 (2006) 112–121
International Journal of Mass Spectrometry
www.elsevier.com/locate/ijms

Ion cluster desorption from frozen NH_3 induced by impact of fast multi-charged ions

R. Martinez [a], C.R. Ponciano [a], L.S. Farenzena [a], P. Iza [a], M.G.P. Homem [b], A. Naves de Brito [b,c], K. Wien [d], E.F. da Silveira [a,*]

[a] *Physics Department, Pontifícia Universidade Católica, Rua Marques de São Vicente 225, 22543-970 Rio de Janeiro, Brazil*
[b] *Laboratório Nacional de Luz Síncrotron, Box 6192, 13084-971 Campinas SP, Brazil*
[c] *Brasilia University, Institute of Physics, Box 04455, 70919-970 Brasília-DF, Brazil*
[d] *Institute of Nuclear Physics, Technical University, 64289 Darmstadt, Germany*

Received 17 January 2006; received in revised form 4 April 2006; accepted 4 April 2006

Abstract

Ion cluster desorption yields due to the impact of ^{252}Cf fission fragments on condensed ammonia are determined. Identification and abundance of the ion desorbed species were provided by a time-of-flight mass spectrometer. Ammonia ice thin layers deposited on Au film were heated from 25 K to complete sublimation. The typical pressure during heating process was 10^{-8} mbar. Measurements in the 25–150 K temperature range show emission of $(NH_3)_nNH_m^{\pm}$ ion clusters, where n varies from 0 to ∼30 and m varies from 0 to 3 (for negative ions) or to 5 (for positive ions). The distribution is described by the sum of two decaying exponentials when n increases, which is interpreted by the simultaneous occurrence of two cluster formation regimes: (i) recondensation of sublimated molecules from the projectile track and (ii) emission of pre-formed bulk fragments from the periphery of the impact site. Moreover, the cluster yields of positive and negative ion series are approximately proportional to each other, suggesting that the ion cluster distribution shape is dictated by the neutral molecules but absolute yield is controlled by the emission of the ion species. In the 125–140 K range, sublimation rate increases, the ice thickness decreases rapidly and all the mentioned cluster series tend to disappear. The series $(HCN)_nCN^-$ then appears, originating in the clustering of residual hydrocarbon contaminants on the metal substrate surface. The residual gases are analyzed as a function of the NH_3 ice target temperature and their partial pressure compared to the ion desorption yield.

PACS: 78

Keywords: Ammonia ion cluster; Secondary ion; TOF; ^{252}Cf-PDMS; Condensed NH_3

1. Introduction

In two recent articles [1,2] we have addressed to the question of whether organic material present in the atmosphere or on the surface of planetary moons could have been produced by electronic sputtering of water ice mixed with carbon dioxide. The experimental method used to identify the new species was time-of-flight (TOF) mass spectrometry of the secondary ions which are part of the flux of particles ejected from ice targets bombarded by MeV heavy ions.

This research is now being extended to other ice mixtures. In particular the mixture of H_2O, NH_3 and CO ices provided an extraordinary complex mass spectrum when exposed to ionizing radiation [3]. Its analysis requires the knowledge of the mass spectra measured for the single ice components, i.e., pure H_2O ice, pure CO ice and pure NH_3 ice as well as of the mass spectrum of mixed NH_3 and CO. Results for pure H_2O, CO and CO_2 have been published [1,2,4]. The present work is focussed on the mass spectra of pure NH_3, which exhibit a pronounced pattern of cluster ions, typical for condensed gas targets.

Ammonia clusters have been the object of several investigations in the last decade [5–9]. The formation of clusters by electronically induced sputtering of low-temperature condensed gas solids (ices) such as water and organic compounds has

* Corresponding author. Tel.: +55 21 3527 1272; fax: +55 21 3527 1040.
E-mail address: enio@vdg.fis.puc-rio.br (E.F. da Silveira).

1387-3806/$ – see front matter © 2006 Elsevier B.V. All rights reserved.
doi:10.1016/j.ijms.2006.04.005

been investigated by a number of researchers (e.g., [2,4,10–14]). Both experimental and theoretical efforts have endeavored to characterize ices of varying compositions formed at very cold temperatures and to elucidate the chemistry that may occur when they are subjected to various environmental regimes [7]. Nucleation processes and cluster formation play a central role, for example, in crystal growth in solution and at interfaces, aerosol formation in the upper atmosphere and particulate formation in the interstellar environment [9]. Theoretical investigations on neutral ammonia cluster structure have been reported as well [15].

In astrophysics, ammonia ices have a particular interest since NH_3 grains are part of atmospheres, cometary surfaces and outer-solar-system bodies which are constantly bombarded by cosmic rays and solar wind [6]. These investigations are closely tied to ongoing instrumental probes and observational studies of ices in the solar system and beyond [7]. Titan, one of Saturn's moons, is of great interest to scientists because it is the only moon known to have clouds and a planet-like atmosphere [16–18]. It is made up primarily of nitrogen, according to observations made by the Voyager spacecraft in the early 1980s. Nowadays, Cassini-Huygens have supplied new evidence about Titan's atmosphere: ammonia released by means of a phenomenon called "cryovolcanism" could be the source of molecular nitrogen [8].

The ammonia molecules possess electric dipole moment and hence it is expected that they polymerize into higher-order neutral $(NH_3)_n$ clusters by *hydrogen-bonding*. A proper theoretical treatment of dipole-bonded neutral agglomerates of ammonia demands an accurate representation of electron correlation [19]. Each of the nitrogen–hydrogen covalent bond in ammonia is formed as a result of the overlapping of one sp^3 orbital of nitrogen with the s orbital of the hydrogen atom. The single non-bonding nitrogen electron pair occupies the fourth sp^3 orbital of the nitrogen. Two N–H bonds form an angle of 107.3° to each other. Nucleation processes and cluster formation have been studied by measuring the relative yields of the $(NH_3)_n$ clusters [20,21]. A predominant population of protonated ammonia clusters has been observed using multiphoton ionization [22–24], single photon ionization [25] and electron impact ionization [26]. Infrared spectroscopy of protonated ammonia clusters [5] and photoionization experiments of neutral ammonia clusters [25] suggest the existence of a central ammonium cation, NH_4^+, similarly to that proposed for protonated water clusters [1].

For ammonia cluster production by sputtering, the crystalline structure of the target ice is expected to play a role in the emission of pre-formed clusters. The simple cubic, hexagonal close-packed and face-centered cubic structures have been determined for solid ammonia at high pressures and temperatures of about 200 K [27,28]. Phase changes of ammonia at high vacuum conditions may be roughly predicted by extrapolating the known NH_3 vapor pressure as a function of temperature [29,30] to lower pressures. Assuming that the ammonia vapor pressure follows an Arrhenius-function for temperatures lower than 170 K, Fig. 1 shows the curve fitted with available data; the dashed region corresponds to the pressure and temperature conditions measured in the current work. However, the sublimation process of

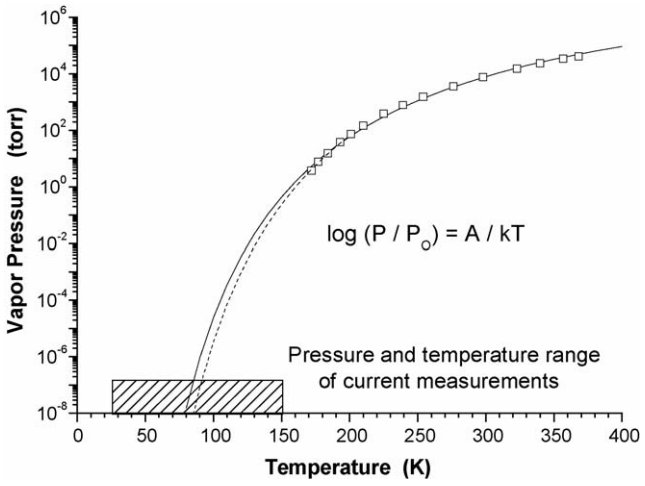

Fig. 1. Dependence of NH_3 vapor pressure on temperature. Data reported for the 172–368 K range from [29,30] was fitted by the $\log(P/P_o) = a/T$ function and extrapolated to lower temperatures (the dashed line corresponds to a smaller number of data points). The marked rectangle indicates typical pressures and temperatures covered in the current work.

ammonia films is a more complex phenomenon. Akbulut et al., using thermal desorption spectroscopy (TDS), found the highest NH_3 desorption rate in the 130–160 K range for coverages decreasing from 1.4 to 0.2 L [31]. Ogasawara et al. reported large release of adsorbed ammonia at 155 K, as well as small TDS peaks at 112 and 125 K due to multilayer and bilayer ammonia, respectively [32]. A 115 K TDS peak was also reported by Benndorf and Madey [33]. Recently, Holt et al. have characterized thin films of solid ammonia by infrared spectroscopy in the 25–110 K temperatures range and for typical pressures of 10^{-6} mbar [34]. They reported three solid phases (amorphous, metastable, and crystalline) for ammonia: the crystalline phase is observed when ammonia is deposited at temperatures above 80 K; the amorphous phase is observed at temperatures below ~50 K and, between 50 and 80 K, the metastable phase is formed.

In this work, ion cluster desorption yields of NH_3 are presented. Ammonia ice is heated from ~25 to 160 K, producing pressures inside analyzing chamber in the 10^{-8}–10^{-6} mbar range. At such experimental conditions, the structure of the condensed ammonia is expected to be simple cubic structure or amorphous. Fast heavy ions are used to produce ion desorption of ammonia clusters. The methods used to identify and characterize the species desorbed from the surface layers are the time-of-flight secondary ion and quadrupole mass spectrometries.

2. Experimental methods

The experiments were carried out at the Laboratório Nacional de Luz Síncrotron – LNLS, Campinas. The analyzing chamber with the experimental set-up, depicted in Fig. 2, was manufactured at LNLS and designed to make in situ analysis of photolysis process in synchrotron light irradiated samples. Following, the experimental techniques are described.

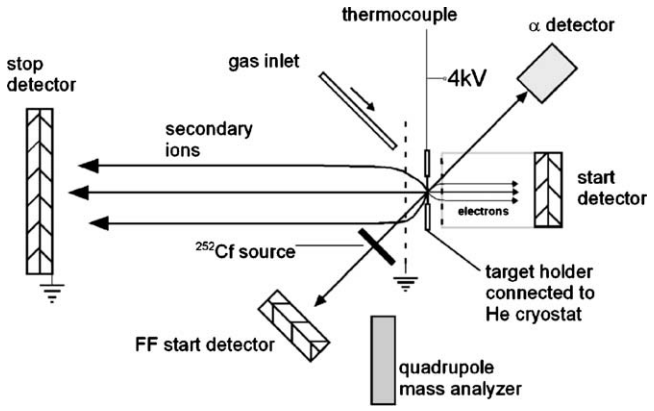

Fig. 2. Experimental set-up used to produce and analyze secondary ions and desorbed neutrals from frozen gases.

2.1. Target preparation

The analyzing chamber is first pumped and backed until the residual pressures decrease down to the 10^{-8} mbar range. Ammonia gas (99.99% pure) is introduced in a pre-chamber (pressure ~100 mbar) and then let flow slowly into the main chamber, whose pressure increases by one-two orders of magnitude. The gas flow is directed towards a thin Au foil (thickness of about 1500 Å) kept at low-temperature by a Cu cold finger connected to a liquid He cryostat (Cryogenic Pump Edwards Model, CH 2/Compressor: Cryodrive 1.5). The temperature of the thin foil holder could be measured by means of a type-K thermocouple capable of monitoring temperature variations of ~1 K; accuracy on the absolute temperature is however considered to be about 2–3 K. As shown in Fig. 2, a cupper thermo-shielding was mounted around the target: it is directly connected to the cold finger and envelops the Au foil, its holder and the thermocouple contact. It is expected that the temperature difference between target and shielding be small, so that the bombarded target site (from where the secondary ions are emitted) should have a uniform temperature, practically equal to that at the thermocouple contact.

Alpha particles of 6.2 MeV from a ^{252}Cf source have been used to determine the thickness of the ice layer being deposited by continuous condensation of the ammonia gas. After crossing the target, the alpha particles are detected by a surface barrier detector and the charge signal is sent to an EG&G Ortec multichannel analyzer. The displacement of energy peak, with the help of energy loss tables, allows the measurement of the ice thickness variation, simultaneously with the acquisition of the mass spectra.

2.2. Secondary ion analysis

A PDMS [35,36] spectrometer was designed and built specially for the mentioned analyzing chamber. Besides having the ability to analyze secondary ions produced by fission fragments (FF) from a ^{252}Cf source, the TOF spectrometer may also analyze those ions produced by (pulsed) synchrotron light irradiation. In this article only data relative to the ^{252}Cf-FF ionization method are considered. The ^{252}Cf source was selected because it offers several experimental advantages: (i) the FF velocities are two or three times higher than Bohr velocity and, therefore, their stopping power is close to the maximum value of the Bragg curve; (ii) since the FF are high-Z elements (such as Ba or Tc) and are emitted as multi-charged ions, their stopping power is very high (in the order of 1 keV/Å passing the ammonia ice); (iii) the radioactive source is very compact, sealed, compatible with ultra-high-vacuum conditions and adequate for the TOF event-by-event measurements; (iv) secondary ion sputtering yields are in the range 0.01–0.1 ions/impact, enabling that a 20 μCi ^{252}Cf source could generate mass spectra of the secondary ions, with reasonable statistics, within a minute of acquisition time. Dependence of desorption yields on target temperature may therefore be followed by mass spectrometry.

The ~60 MeV ^{252}Cf-FF impinge on the front side of the target at an angle of 45° (see Fig. 2). They traverse first the ice layers and then the target substrate, the thin gold foil. Note that the two simultaneous FF are emitted in opposite directions, one towards the target and the complementary one towards the FF start detector. In this arrangement, the secondary ions are backward (with respect to the incident beam) ejected from the ice layer and are accelerated towards the stop detector equipped with two microchannel plates.

The start signals are generated by two detectors available in the system: (i) the FF signal is produced by the detection of one of the two FF emitted by the ^{252}Cf source; (ii) the e^- start signal is given by the secondary electrons produced at the target backside by the complementary FF leaving the Au foil; the electrons are accelerated to about 2 keV and detected by a second channel plate assembly. The first type of start signals is used for thick target measurements (in which case the FF cannot traverse them) and the second one is chosen when good mass resolution is needed. For absolute secondary yield measurements, a coincidence of these two signals is required to eliminate false counts.

The impact of FF on the target induces desorption of positive and negative ions, as well as neutral particles. The desorbed ions are accelerated by the extraction field towards the drift region and are detected by the stop detector. Negative and positive ions can be measured sequentially by reversing the high voltage polarity. Further description of the TOF technique is provided elsewhere [37,38].

2.3. Analysis of the neutral species desorption

The residual gases in the analyzing chamber are monitored by a quadrupole mass spectrometer [39] manufactured by Balzers Prisma, Model QME 200. This instrument ramps the mass/charge ratio in the 1–100 u/e range during a preset time and stores the corresponding ion current. After a number of cycles it is possible to visualize how the residual gas mass spectrum evolves over time. Furthermore, as the ice temperature value is periodically recorded, a tri-dimensional plot shows how the ion current of each filtered ion in the quadrupole analyzer (proportional to the partial pressure of the corresponding residual gas) varies as the ice temperature increases.

Residual gases in the analyzing chamber are formed by the sublimated species from the ice, by the atmospheric gases H_2, H_2O, N_2 and O_2, as well as by the organic molecules originated from the pump oil. At equilibrium and because the temperature of the chamber wall does not vary much, their partial pressures are about constant in time. When the target temperature is set to vary, the rate of the ice sublimation may vary dramatically, changing the residual gas composition monitored by the quadrupole spectrometer. Unfortunately, the residual gas partial pressures are related to the average rate desorbed species of all internal parts of the chamber and not only to desorption rate of the target. Because of this fact, the analysis of the neutral species desorption is not as straightforward as the secondary ion mass spectrometry in the sense that the ions do come from a specific spot in the target (defined by the collimated FF beam) whereas the neutral species come mainly from spots undergoing phase transition in the target holder system, which not necessarily are at the target temperature. Monitoring the residual gas pressure is relevant because – besides the influence of the intense rate desorption of neutrals on the ion emission – the increase of pressure in the chamber may interfere in the detection of secondary ions.

3. Experimental results

As a general procedure, the target temperature is cooled down to ~25 K, the cryostat is turned off and then the ice, target holder and cold finger warm up to ~160 K by natural heat exchange. The secondary ion emission from the frozen NH_3 and the residual gas data were simultaneously acquired in this temperature range. It was pointed out in the previous section that ion mass spectra can be correlated with precise ice temperatures while mass spectra of residual gases cannot.

3.1. Time-of-flight spectra

NH_3 ice mass spectra of positive and negative secondary ions in the 0–500 u range are presented in Figs. 3 and 4, respectively. Each inset shows details in the 0–100 u mass range.

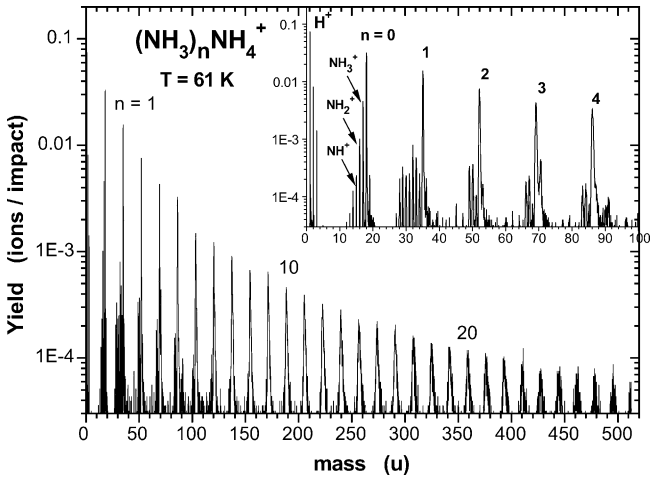

Fig. 3. Positive ion mass spectrum of NH_3 ice at 61 K, irradiated by FF during 1 h.

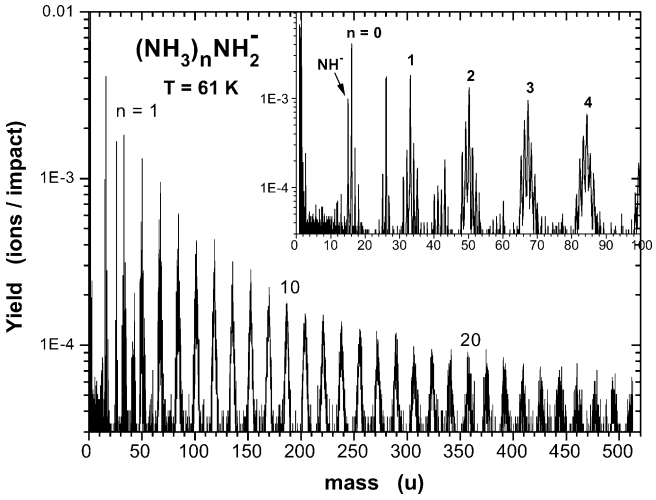

Fig. 4. Negative ion mass spectrum of NH_3 ice at 61 K, irradiated by FF during 1 h.

3.1.1. Positive ions

The PDMS TOF mass spectrum of secondary ions emitted by the NH_3 ice (see Fig. 3) is characterized mainly by the $(NH_3)_nNH_4^+$ ammonia cluster ion series with $n=1$ to $n>30$. Such a distribution is very similar to that emitted by H_2O ice FF bombardment [13]. It will be shown later that the mass dependence of the $(NH_3)_nNH_4^+$ yields is described by the sum of two exponential decaying functions. Note also that each cluster peak of order n is in fact a group of six mass peaks: (i) the dominant peak corresponds to the $(NH_3)_nNH_4^+$ ions; (ii) from its lower mass side, four satellite peaks are formed by the loss of one to four H atoms by the NH_4^+ ion, that is, the $(NH_3)_nNH_m^+$ series, where m varies from 0 to 3; (iii) from the higher mass side of the dominant peak, there appears another satellite peak smaller by one order of magnitude and heavier by one mass unit, corresponding to the $(NH_3)_nNH_5^+$ [40,41]. This series formed with these heavier satellite peaks should correspond to the $(NH_5)_n^+$ or – less likely – to $(NH_3)_nH_3O^+$ structures. The designation $(NH_3)_nH_3O^+$ naturally requires the presence of oxygen, which may be supplied by condensed H_2O (instead of O_2, see discussion in Section 3.3).

The low mass region of the spectrum is shown in the inset of Fig. 3. At the right side of the three hydrogen peaks, it is visible the C^+ and the CH^+ peaks as well as the $n=0$ ammonia group, which is formed by the 6 positive ions mentioned: N^+, NH^+, NH_2^+, NH_3^+, NH_4^+ and NH_5^+. Peaks at mass 18 and 19 u may have some contribution of water peaks [13]: the former (H_2O^+) is overlapped with the overwhelming NH_4^+ peak and the latter is attributed mostly to NH_5^+ (with some contribution of H_3O^+). The next group of peaks is composed mainly by: N_2^+ (mass 28 u), N_2H^+ (29 u), $NO^+ + N_2H_2^+$ (30 u), the five $n=1$ $(NH_3)NH_m^+$ peaks (31–35 u)-including O_2^+ (32 u), and the 36 u mass peak, i.e., $(NH_3)_2H_2^+ + (NH_3)H_3O^+$. Analysis of the following group gives: $(NH_3)N_2^+$ (45 u), $(NH_3)O_2^+$ (47 u), $(NH_3)_2NH_m^+$ and $(NH_3)_3H_2^+ + (NH_3)_2H_3O^+$ (51 u).

3.1.2. Negative ions

The same pattern described for the positive ion clusters is also observed for the negative ones. The PDMS-TOF mass spectrum of Fig. 4 shows groups of peaks with decreasing yield as the cluster mass increases. The de-protonated species NH_2^- are one of the most abundant ions in the desorption process, coming from the $NH_3^* \rightarrow NH_2^- + H^+$ fragmentation, and are responsible for the dominant series $(NH_3)_nNH_2^-$. The fragmentation $NH_3^* \rightarrow NH^- + H_2^+$ or $NH_2^* \rightarrow NH^- + H^+$ are also likely to occur and should generate the $(NH_3)_nNH^-$ negative ion series. Electron capture by a free N atom or by a neutral ammonia cluster should produce the $(NH_3)_nN^-$ or the $(NH_3)_n^-$ series, respectively. These processes justify the group of negative cluster ion series $(NH_3)_nNH_m^-$, where m varies from 0 to 3, observed in the inset of Fig. 4. Note that the typical yields of negative ammonia ions are about one order of magnitude lower than that of the positive ones. In Section 3.2 it will be shown that, similarly to the positive ion yields, the ammonia negative ion yields decrease with n according to the sum of two exponentials.

Contaminants are responsible for the OH^- and C_2^- peaks observed at 17 and 24 u, respectively. Note the particularly intense CN^- anion hybrid peak at mass 26 u, which suggests that CNO^- could be the mass 42 u peak. The N_3^- (azide anion) and HN_3^- species are also candidates for the peaks corresponding to masses 42 and 43 u, respectively.

3.2. Cluster yield dependence on nuclearity

Cluster nuclearity, n, is defined as the number of the cluster constituents. In the case of ammonia clusters, this parameter is understood as the number of NH_3 molecules linked together and attached to the radical $R^{+(-)}$ forming the ion cluster. Only the dominant series, $(NH_3)_nNH_4^+$ for positive and $(NH_3)_nNH_2^-$ for negative ion clusters, will be considered for this analysis.

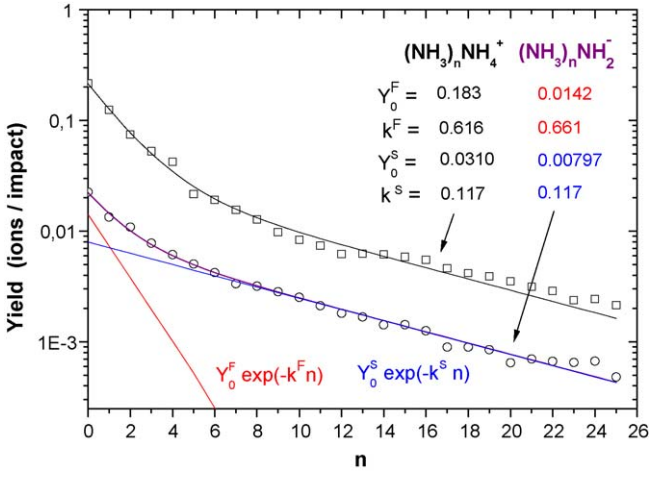

Fig. 5. Dependence of the cluster yield of the positive and negative ammonia ions on the nuclearity n, the number of NH_3 molecules. Note that the curves are nearly parallel to each other in this semi-log plot, i.e., the positive ion yield distribution is nearly proportional to the negative one. The solid lines were obtained by fitting data with Eq. (1). The obtained slope parameters are shown; $A_F/A_S = 5.9$ and 1.8 for the positive and negative ion series, respectively. The contributions due to the fast and the slow regimes for the $(NH_3)_nNH_2^-$ distribution are depicted.

Fig. 5 presents the cluster ion desorption yields, for 61 K ammonia ice, obtained from the mass spectra of Figs. 3 and 4 as a function of n ranging from 1 to 25. As data are displayed in a semi-log plot, the two obvious observations are that the positive and negative ion yields are proportional to each other and that the dependence on n is not exponential. Nevertheless, since the points are practically aligned at the low-n and high-n regions, the yields should be described by the sum of two exponentials.

Indeed, the two solid lines shown in the plot were calculated from the expression

$$Y = Y_0^F \exp(-k^F n) + Y_0^S \exp(-k^S n), \quad (1)$$

where Y_0^F and k^F are the yields for $n = 0$ and the slope coefficients relative to the fast (F) decay regime, respectively; Y_0^S and k^S are the corresponding parameters for the slow (S) decay regime. The agreement with the current experimental data is very good and the physical meaning of this expression is attributed to the contribution of two distinct mechanisms of cluster formation.

3.3. Temperature variation

Continuous acquisition of mass spectra was made during the warming up of the ammonia ice target, except for the 95–104 K and 118–128 K temperature ranges, when the desorption yield was too intense and the stop detector became saturated (data suppressed). The dependence of the $(NH_3)_nNH_4^+$ yields on the ice temperature (60–150 K) is shown in Fig. 6 where only clusters with $n = 0$–4 or multiples of 4 are represented; the main observed characteristics are presented, with their respective interpretation:

(i) yields are about constant for small clusters ($n < 4$) up to ~100 K, suggesting that they are most produced in a locally hot region (track) of the target, which temperature is not influenced by the average ice temperature;

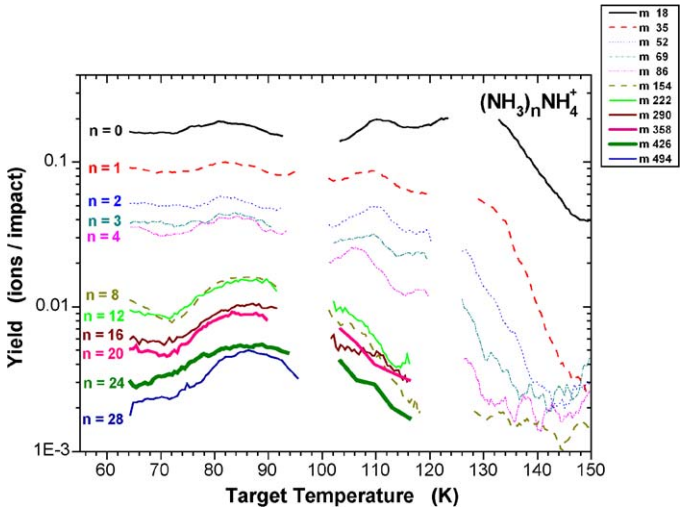

Fig. 6. Plot of the intensities of the $(NH_3)_nNH_4^+$ ion clusters versus target temperature. Data is suppressed in the 95–104 K and 118–128 K temperature ranges due to intense ice sublimation causing ion detection problems. For clarity, for $n > 4$, only yields of clusters with n multiple of 4 are plotted.

(ii) yields of small clusters have a modest increase for $T = 75$–85 K; these clusters would be emitted from a cold region (around the track) and may be correlated with a metastable phase such as the one reported to occur between 50 and 80 K [34];
(iii) this yield increase is more evident for large clusters, suggesting that they are produced mainly at the cold regions where effects of the bulk structure are noticeable;
(iv) above ∼110 K, the NH_4^+ ion yield starts to increase while those of all the other ion clusters decrease, an evidence that – near sublimation or for very thin ice layers – the formed ion clusters tend to dissociate releasing the NH_4^+ ion;
(v) small yield structures appear for $n = 2$, 3 and 4 close to 110 and 120 K; one may tentatively associate these maxima with the 112 and 125 K TDS peaks reported by Ogasawara [32];
(vi) at last, in the 130–150 K range, all the ammonia ion yields decrease rapidly showing that the ice layer vanishes.

Another way to represent the same data is depicted in Fig. 7, where the ammonia cluster yields are plotted as a function of nuclearity for 4 ice temperatures. The regimes of fast and slow-decay (Eq. (1)) are clearly observed for the different temperatures, with some variations in the range of temperatures measured. The general trend for all ion cluster yields is that they are low for low temperatures (70 K), have a maximum at 80–85 K, close to the sublimation temperature, and then decrease afterwards (110 K) because the ice layer is disappearing. Note that the dominant mechanism responsible for the formation of small clusters is not sensitive to temperature, while the one for the large clusters is. In terms of Eq. (1), this means that: (i) Y_0^S is a function of the ice temperature while Y_0^F is not and (ii) $Y_0^F \gg Y_0^S$.

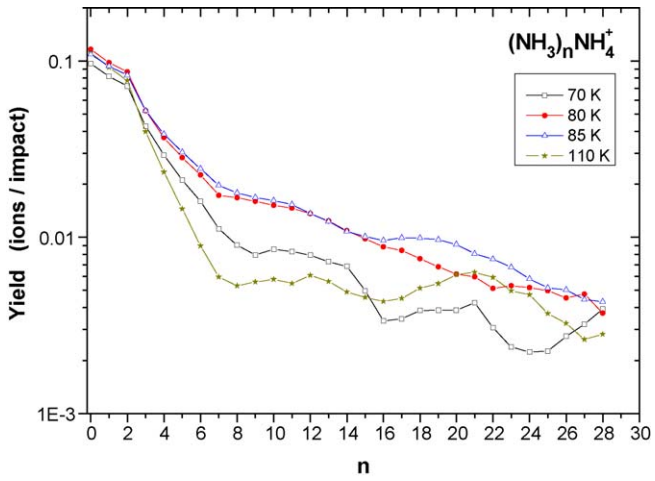

Fig. 7. $(NH_3)_nNH_4^+$ ion cluster yields as a function of the nuclearity n, at different ice temperatures. Remind that – in the TOF technique – data for all n are acquired simultaneously. The yields of small ion clusters are not very sensitive to the target temperature, while those of the large clusters are.

The temperature variation effects were also followed by the quadrupole mass spectrometer measurements. Phase transitions of solid ammonia are supposed to occur at 50 K (from crystalline to metastable) and at 80 K (from metastable to amorphous). Sublimation should also occur at ∼80 K for 10^{-8} mbar pressures (see Fig. 1). Our results, obtained with the quadrupole spectrometer and displayed on the 3D diagram (ionic current versus ion mass and target temperature), are shown in Fig. 8. Ammonia

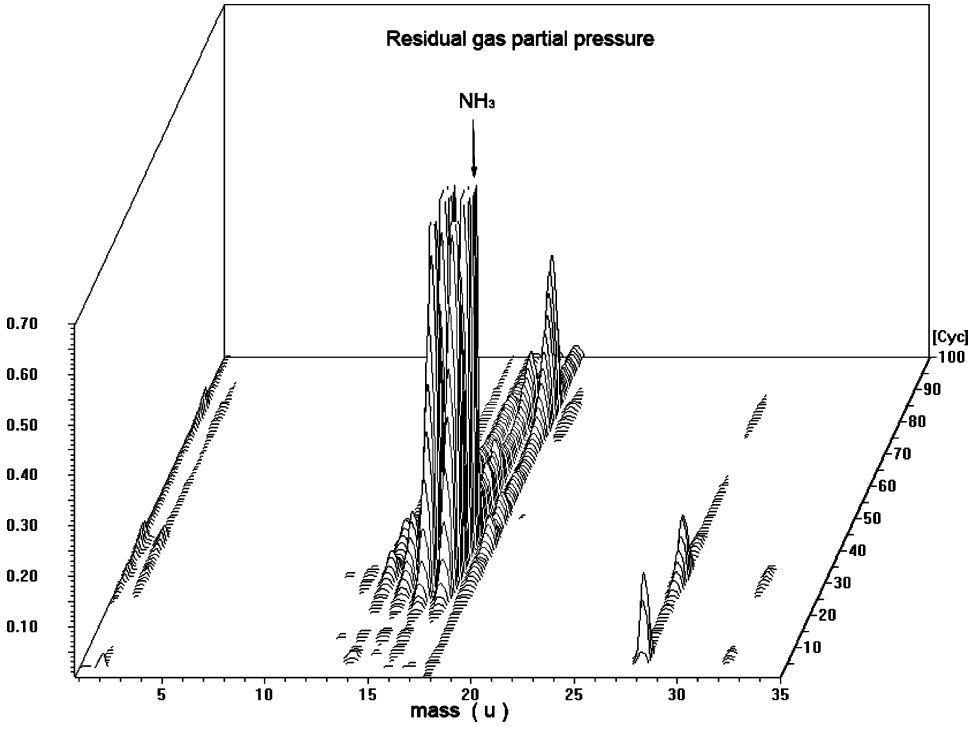

Fig. 8. Quadrupole mass spectra of the residual gas during the target warming up. The vertical axis represents, in arbitrary units, the ion current through the quadrupole, (which is proportional to partial pressure of the parent neutral molecules). The horizontal axis represents the mass of the ions traversing the quadrupole filter and the third axis the warming up time (cycles of the quadupole).

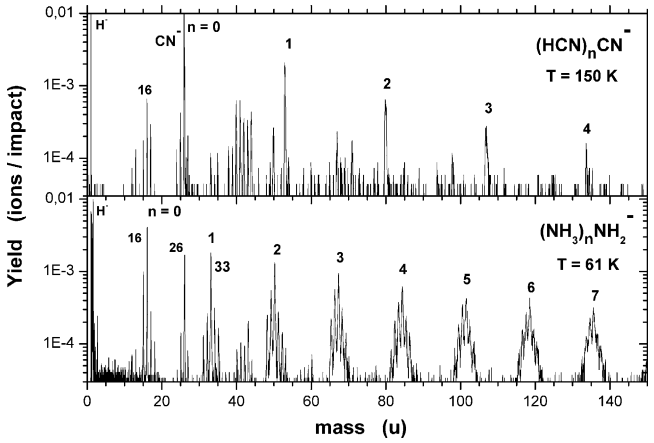

Fig. 9. Comparison of negative ion mass spectra obtained at temperatures below (at $T = 61$ K, lower figure) and above (at $T = 150$ K, upper figure) the ammonia ice sublimation temperature (~80 K, at UHV pressures). The series $(NH_3)_nNH_2^-$ characterizes the ammonia ice layer as target while the appearance of the HCN^- and CN^- peaks indicates that the ice layer has vanished.

sublimation at ~80 K is observed by the rapidly increasing current of ions having masses 17, 16, 15 and 14 u (NH_3^+, NH_2^+, NH^+ and N^+). Peaks at masses 1, 2 and 28 are attributed to H^+, H_2^+ and N_2^+, probably originated from H_2, and N_2 trapped in ammonia ice and/or formed in the quadrupole head by electron impact on NH_3. Note that all these peaks exhibit the same temperature dependence. A very small O_2^+ peak due to trapped O_2 appears at ~80 K. Sublimation of ammonia is clearly separated from that of water: the ion intensities of the NH_m^+ group practically disappear for temperatures above 145 K, while the H_2O^+ peak shows a maximum around 155 K. The H^+ peak visible at 115 K is attributed to water molecule fragmentation.

3.4. The $(HCN)_nCN^-$ series

The vanishing of the ice layer is confirmed by the dramatic changes in the negative ion mass spectra acquired above 150 K, as shown in Fig. 9: the dominant $(NH_3)_nNH_2^-$ series disappears while a new and intense $(HCN)_nCN^-$ series shows up. The presence of the carbon atom is attributed to residual hydrocarbon contaminants, particularly on the metal substrate surface. This finding is interesting since it reveals the high production yields of new compounds (e.g., HCN^-, CN^-) originated from FF induced chemical reactions of ammonia with hydrocarbon contaminants; such a behavior might help the interpretation of mass spectrum peaks of ice mixtures, e.g., NH_3 and CH_4, which are common constituents of comet's surfaces.

The interpretation of the $(HCN)_nCN^-$ series formation is supported by a number of arguments. Considering that only H, C, N and O are the elements with relevant abundance in the target surface, the dominant peak corresponding to mass 26 u in the negative ion spectrum (Fig. 9, upper) must be attributed to CN^-. The masses of other members of the dominant series are obtained by adding to 26 a multiple of 27, indicating that this value is the mass of the neutral cluster monomer. The presence of the oxygen in a 27 u molecule is again promptly excluded, leaving three possible molecular structures: HCN, HNC and C_2H_3. The latter molecule is not stable and the hydrogen isocyanide, HNC, is a rare compound usually produced from glow discharges in the hydrogen cyanide, HCN [42]. Therefore, the assignment $(HCN)_nCN^-$ is the most likely for such series of peaks. Inspection of the smaller peaks in the same spectrum revels that some of them can be attributed to the $(HCN)_nNH_3^-$ and $(HCN)_nCH^-$ series; the other are due to the disappearing $(NH_3)_nNH_m^+$ series and to a relatively small contribution of water (mass 35 u peak may be due to the $(H_2O)OH^-$ ion). Furthermore, it is well known that HCN polymerizes and that its formation is extremely fast when it is chemically possible [43].

4. Discussion

Analysis of the positive and negative mass spectra of ammonia ice reveals that the ion masses corresponding to the observed peaks may be sorted into series having the structure $(NH_3)_nR^+$ or $(NH_3)_nR^-$, where R are atomic or molecular ions, e.g., H^+, H_2^+, H_3O^+, NH_m^+, H^- and NH_m^-. Such designation fit very well for two different cluster emission processes. In one scenario, it is assumed that part of the bulk is fragmented by the projectile into molecules, atoms and ions. Once emitted, these neutral molecules start to condense preferentially around the ion radicals $R^{+(-)}$. The relative total yield of each series $(NH_3)_nR^{+(-)}$ is then proportional to the relative desorption yields of the each $R^{+(-)}$. The yield distributions on n for the different R's depend on the agglutination rate of the neutrals. It is proposed here that this is the mechanism responsible for the fast-decay regime (F).

Another scenario is the emission of pre-formed clusters. They may be emitted already ionized or be ionized in-flight. In the first case, "shanks" are produced by shock waves and are ionized by secondary electrons. In the other case, the $(NH_3)_n$ clusters are emitted excited, loose an electron, cool down in the time scale of 10^{-14}–10^{-13} s, with eventual "boiling off" of some NH_3 molecules (or a molecular fragment), while a proton migration forms the central NH_4^+ ion [25]. Anion clusters, formed by electron capture, undergo into a similar evolution. Such mechanisms would be responsible for the slow-decay regime (S).

4.1. $(NH_3)_nNH_4^+$ or $(NH_3)_{n+1}H^+$?

Two arguments favor the $(NH_3)_nNH_m^+$ structure: (i) the observed red-shift of the N–H stretching modes of the NH_4^+ core [5] and (ii) theoretical results show that this structure is the most stable one [19]. Indeed, infrared spectroscopy of protonated ammonia clusters $(NH_3)_{n+1}H^+$ has shown that there are strong absorption bands due to a central ammonium NH_4^+ cation and weaker bands due to the remaining neutral ammonia clusters, so that the cluster structure would be better described as $(NH_3)_nNH_4^+$ [5]. Such structure is analogous to that proposed for protonated water clusters [1,13]. On the other hand, the NH_4^+ core argument may be questioned for clusters formed by very fast electronic sputtering: it is worth pointing out that, in the current experiments, the quartets obtained by Pfeiffer et al. [9] are not observed, probably because the experimental conditions are different (they used electron impact ionization at ambient temperature).

In favor of the $(NH_3)_{n+1}H^+$ structure, in which the H^+ ion would be at the cluster periphery and not in the core, there is attachment scenario mentioned above. In particular, the designation of a $(NH_3)_{n+1}H_2^+$ series is compatible with the existence of a $(NH_3)_{n+1}H^+$ series as the main cluster structure, since the H_2^+/H^+ and the $(NH_3)_nH_2^+/(NH_3)_nH^+$ desorption yield ratios are the same (about 0.1). To illustrate research on similar clusters, Nguyen et al. [44], analyzing gas phase hydrates of alkylammonium ions, claim that these structures are formed by attachment to an external water cluster rather than by a central ion structure.

4.2. Yields of positive and negative ions

Figs. 3 and 4 show typical positive and negative secondary ion TOF spectra of frozen NH_3 irradiated by ^{252}Cf-FF of ~60 MeV. The yields of the positive ion series are one order of magnitude higher than the yields of the negative series, which is ultimately due to the electronic sputtering process. A large number of secondary electrons is pushed away from the impact region, creating more positive ions than negative ones. Moreover, a fraction of these is retained by the positive track produced in the target, while the positive ions are strongly repelled, becoming less likely to be neutralized in-flight by electron capture. The existence of negative secondary ions must be a consequence of a very high ion production rate and/or a large electron affinity. As an example, the electron affinity of CN^- is 3.862 eV [30], one of the highest values found for compounds.

4.3. Cluster yields as a function of n and T

The yield distributions of the $(NH_3)_nNH_4^+$ cluster series can be fitted quite well by a sum of two exponential functions (Eq. (1)). The two slope parameters, k^F and k^S, and the fast-slope cluster-head yield, Y_0^F, are found to be not very sensitive to temperature while the slow-slope cluster-head yield, Y_0^S, is. Indeed, from Figs. 6 and 7 and Table 1, it is observed that, warming up and close to the sublimation temperature (50–80 K), the production rate or stability of large positive ion clusters is more affected than that of small ones. The double exponential behavior has already been reported for other ices bombarded by heavy ions in high stopping power conditions [13,45]. The parameter Y_0^F was found to be constant for water ice when temperature was varied from 80 to 150 K [13]. Matsuo et al. [46], using MeV Ar ions on water ice, attributed the deviations from the monotonic decrease in the cluster distribution to the high stability of certain clusters.

Table 1
Fast (F) and slow (S) slope parameters for 61 K for ammonia and water ion cluster series ($k_m = k/M$, where M is the monomer mass)

	Temperature (K)	k^F	k^S	k_m^F	k_m^S
$(NH_3)_nNH_4^+$	61	0.62	0.12	0.036	0.007
$(NH_3)_nNH_2^-$	61	0.66	0.12	0.39	0.007
$(H_2O)_nH^+$	80	0.81	0.14	0.045	0.008
$(H_2O)_nOH^-$	80	0.63	0.16	0.035	0.009

Results are compared with the corresponding parameters for water [9].

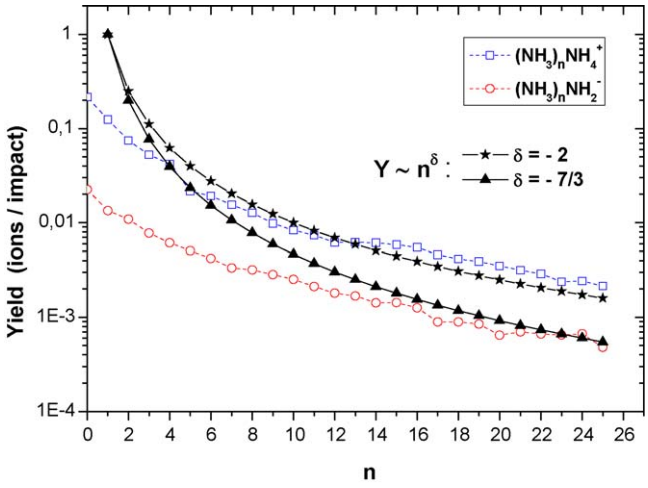

Fig. 10. Comparison of the experimental data (open symbols) obtained in this work with predictions of the hydrodynamical model developed in Ref. [36].

It is also worthwhile to note that Lancaster et al observed just one exponential for water ice clusters up to $n \sim 20$, when bombarded with 0.5–3 keV He^+ ions [47]. For these three experiments with water ice, it was found $k^s \sim 0.14$, a value approximately equal to that determined in the current work for ammonia ice.

It is worthwhile to analyze the behavior of non-condensed gas targets. Boudjadar et al. reported the size-distribution of the cluster ion yields of uranium dioxide by using fast (11 MeV/u Kr^{32+}) and slow (83 keV Th^{75+} and 81 keV Xe^{23+}) projectiles [48]. They proposed, for both velocity regimes, that UO_2 clusters can be described by a power law $Y \sim n^{-\delta}$, with δ values between 1.5 and 2.9, in agreement with the predictions of collective ejection models, in particular with the hydrodynamical (phase transition) model [49], which successfully predicts $\delta = 7/3$. However, since their data covers only $n \leq 8$, an exponential behavior is also acceptable, yielding $k^F \sim 0.6$, about the same value for the ammonia clusters. The inverse is not true: the current positive or negative ion ammonia clusters are not correctly described by the power law distribution (Fig. 10), suggesting that the hydrodynamical models are not appropriated for the ammonia cluster distribution.

The exponential behavior of the ion cluster distribution obtained by the current measurements on ammonia clusters indicates that data should be better described by the "statistical models" [44] which are developed for processes in which there occurs a re-aggregation of individual atoms upon or after ejection [50–53].

Supplementary information on ammonia cluster stability can be obtained from inspection of ion clusters not produced from ice. Results on this property were reported by Pfeiffer et al. by using electron impact ionization of a supersonic molecular beam of neutral ammonia clusters [9]. They observed a population distribution of the ion clusters $(NH_3)_{n-1}NH_2^+$ and $(NH_3)_nH_2^+$ which is nor exponential neither potential law, evidencing formation through another type of process (Fig. 11). Furthermore, the magic number $n = 7$ was found, indicating an associative ion-molecule reaction between an NH_2^+ daughter ion and an NH_3 solvent molecule.

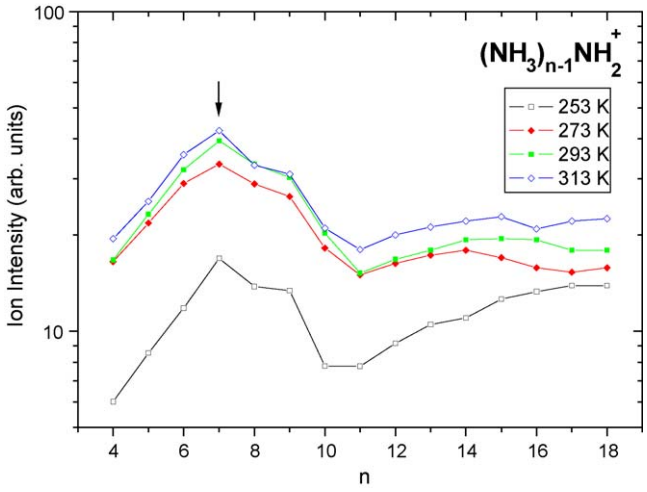

Fig. 11. Distribution of the ion clusters $(NH_3)_{n-1}NH_2^+$ produced via electron impact ionization of a supersonic molecular beam of neutral ammonia clusters [5].

The yields for negative ion clusters $(NH_3)_nNH_2^-$ can also be fitted, in good approximation, by a sum of two exponential functions (Fig. 7); the corresponding slope parameters k are also shown in Table 1 for 61 K. If only $n = 0$–5 members are considered, $k^F \sim 0.661$; for $n > 5$, $k^S \sim 0.117$. It is worth noting that the k parameter is about the same for both negative and positive cluster series produced by FF. This suggests the same formation mechanism, although the survival probabilities be different by one order of magnitude. Comparison among the slope parameters obtained for ammonia and those for $(H_2O)_nH^+$ and $(H_2O)_nOH^-$ cluster yields, measured at the same conditions, shows that they are about the same, enhancing the suggestion that the same basic desorption mechanism is occurring [46].

5. Cluster emission model

The findings of the current work and of the referred articles are consistent with a cluster emission model based on two simultaneous and independent regimes:

(i) The *recombination regime* (F-regime) occurs very close to the infratrack, where temperature is high compared to the ice temperature (which accounts for this process not be sensitive to the ice temperature). The bulk sublimates completely in the infratrack, at least in a region close to the surface where local pressure cannot be too high due to material emission into vacuum. The F-regime causes molecular fragmentation into atoms and/or ions. The gas expansion produces condensation, but the high emission velocities (~ 30 km/s) and the relatively small quantity of ejecta (thousands of atoms) constitute an environment for inefficient production of large clusters (which accounts for the fast decreasing slope distribution, i.e., large k^F values). It is expected that condensation is more efficient when the starting seed is an ion instead of a neutral molecule (binding energy of ion-neutral particles is higher than neutral–neutral ones: attractive polarization effects are enhanced especially for small molecules). The absolute yield of a cluster series characterized by a ion radical R is proportional to the density of R in the gas phase. The growing rate of positive ion clusters is about the same as the negative ones since both depend equally on the attachment probabilities of neutral molecules (which accounts for the desorption yield distribution of positive species be proportional to the negative one). The cluster structures are determined by the condensation process, i.e., the most favorable thermodynamical configuration. This regime only occurs when a high temperature track is formed, situation that depends in particular on the projectile stopping power in the ice. Light projectiles having stopping power lower than a certain threshold do not induce ion desorption in the F-regime.

(ii) The *fragmentation regime* (S-regime) occurs in a colder region around the infratrack, so that the corresponding sputter yields depend on the ice temperature and on the bulk structure. The S-regime is not very destructive, i.e., small and large fractured parts of the solid are pushed way from the surface, giving rise of neutral, positive or negative charged clusters. The cluster structures resemble the bulk structure, since "crystalline" memory is preserved. The total cluster yield increases with the stopping power value but the solid fragmentation pattern is rather insensitive to it, in the sense that the cluster yield distribution shape (the k^S-slope) are fairly the same. It is expected that the charges of the fractured parts are generated along the fracture lines, but during MS analysis (in the μs time range), charge migration and structural change may happen to excited clusters, driving transitions into the more stable configurations produced in the F-regime. Molecular "boiling off" may also occur at this stage of de-excitation, as well as fragmentation of very excited large clusters into smaller ones.

6. Conclusions

In this work, the yields of the positive and negative ion clusters emitted from frozen ammonia bombarded by fission fragments were analyzed. The observed cluster yield distributions for positive and negative ion series do not show expressive indication of magic numbers. Instead, their decreasing yields as the cluster mass increases are well fitted by the sum of two exponentials: one describes a fast-slope (F) regime and the other one corresponds to a slow-slope (S) regime. The ion cluster yield contribution for the S-regime depends on the ice temperature while the one for the F-regime does not. Both the F and S negative ion cluster yield distributions are proportional to the positive ones, giving a strong argument that processes for positive and negative ion clusters and are the same.

These observations support a model based on two simultaneous but not ubiquitous processes: recombination and fragmentation processes, which are associated to the F- and S-regimes, respectively. The recombination process occurs very near to the track core while the fragmentation one occurs peripherically.

Cluster structural stability seems not to play a fundamental role, since the observed distribution is mainly attributed to the

process of cluster formation. Whenever the target temperature increases, approaching the ice sublimation for vacuum conditions, dissociative process becomes more important and the population of all large cluster decreases, enhancing strongly the emission of the ion monomer (NH_4^+ in this case).

More theoretical work is needed to describe the ion cluster emission. The so called statistical models predict exponential law distributions considering the molecular sublimation followed by dynamical re-aggregation in a region very close to the impact site. This situation corresponds to the F-regime. However, collective models describing the emission of "shanks", which corresponds to the emission in the S-regime, predict a power law distribution which is not observed for the condensed gas targets.

Acknowledgements

The authors would like to acknowledge the Brazilian Agencies CNPq, Faperj and Fapesp for their support. P. Iza thanks CLAF for his scholarship. The LNLS staff is acknowledged for support during the experiments.

References

[1] L.S. Farenzena, V.M. Collado, C.R. Ponciano, E.F. da Silveira, K. Wien, Int. J. Mass Spectrom. 243 (2005) 85.
[2] C.R. Ponciano, L.S. Farenzena, V.M. Collado, E.F. da Silveira, K. Wien, Int. J. Mass Spectrom. 244 (2005) 41.
[3] M.G.P. Homem, R.R.T. Marinho, F. C. Gozzo, C.R. Ponciano, E.F. da Silveira, M.N. Eberlin, O. Björneholm, A. Naves de Brito. The 14th International Conference on Vacuum Ultraviolet Radiation Physics, Abstract p. 62, Cairns, Australia, July 19–23, 2004.
[4] L.S. Farenzena, R. Martinez, P. Iza, C.R. Ponciano, M.G.P. Homem, A. Naves de Brito, E.F. da Silveira, K. Wien, Int. J. Mass Spectrom. 251 (2006) 1.
[5] R.L. Johnston, Atomic and Molecular Clusters Taylor and Francis, London, 2002 pp. 71.
[6] R.E. Johnson, Energetic Charged Particles Interaction with Atmospheres and Surfaces, Springer-Verlag, Heidelberg, 1990.
[7] D.E. Won, Icarus 149 (2001) 277.
[8] R.D. Lorenz, J.I. Lunine, Icarus 122 (1996) 79.
[9] W.R. Pfeiffer, M.T. Coolbaugh, J.F. Garvey, J. Chem. Phys. 91 (11) (1989) 6684.
[10] M. Wagner, K. Wien, B. Curdes, E.R. Hilf, Nucl. Instr. Meth. B 82 (1993) 362.
[11] R.L. Betts, E.F. da Silveira, E.A. Schweikert, Int. J. Mass Spectrom. 145 (1995) 9.
[12] K. Wien, C.S.C. de Castro, Nucl. Instr. Meth. B 146 (1998) 178.
[13] V.M. Collado, L.S. Farenzena, C.R. Ponciano, E.F. da Silveira, K. Wien, Surf. Sci. 569 (2004) 149.
[14] H. Tawara, T. Tonuma, H. Kumagai, T. Matsuo, J. Phys. B 27 (1994) 127.
[15] S.A. Kulkarni, R.K. Pathak, Chem. Phys. Lett. 336 (2001) 278.
[16] J.I. Lunine, Adv. Space Res. 10 (1990) 137.
[17] P.A. Gerakines, W.A. Schutte, P. Ehrenfreund, Astron. Astrophys. 312 (1996) 289.
[18] R.D. Lorenz, S.E. Shandera, Geophys. Res. Lett. 28 (2001) 215.
[19] F.A. Fernandez-Lima, C.R. Ponciano, M.A. Chaer Nascimento, E. F. da Silveira, J. Phys. Chem. B, submitted for publication.
[20] J.A. Odutola, T.R. Dyke, B. Howard, J.S. Muenter, J. Chem. Phys. 70 (1979) 4884.
[21] S. Süzer, L. Andrews, J. Chem. Phys. 87 (1987) 5131.
[22] S. Wei, W.B. Tzeng, A.W. Castleman Jr., J. Phys. Chem. 92 (1990) 332.
[23] S. Wei, W.B. Tzeng, A.W. Castleman Jr., J. Phys. Chem. 93 (1990) 2506.
[24] S. Wei, K. Kilgore, W.B. Tzeng, A.W. Castleman Jr., J. Phys. Chem. 95 (1991) 8306.
[25] H. Shinohara, N. Nishi, N. Washida, J. Chem. Phys. 83 (1985) 1939.
[26] C. Lifshitz, F. Louage, J. Phys. Chem. 93 (1989) 5633.
[27] Y. Enginer, S. Salihoglu, H. Yurtseven, Mater. Chem. Phys. 73 (2002) 57.
[28] R.L. Mills, D.H. Liebenberg, Ph. Pruzan, J. Phys. Chem. 86 (26) (1982) 5219.
[29] http://www.airliquide.com/.
[30] D.R. Lide (Ed.), Handbook of Chemistry and Physics, 76th ed., CRC Press, Boca Raton, 1995–1996.
[31] M. Akbulut, N.J. Sack, T.E. Madey, J. Chem. Phys. 103 (1995) 2202.
[32] H. Ogasawara, N. Horimoto, M. Kawai, J. Chem. Phys. 112 (2000) 8229.
[33] C. Benndorf, T.E. Madey, Surf. Sci. 135 (1983) 164.
[34] J.S. Holt, D. Sadoskas, C.J. Pursell, J. Chem. Phys. 120 (15) (2004) 7153.
[35] R.D. Macfarlane, D.F. Torgerson, Science 191 (1976) 920.
[36] K. Wien, Nucl. Instr. Meth. B 131 (1997) 38.
[37] P. Hakansson, Braz. J. Phys. 29 (3) (1999) 422.
[38] M. Guilhaus, J. Mass Spectrom. 30 (1995) 1519.
[39] M.J. Drinkwine, D. Lichtman, Partial Pressure Analyzers and Analysis, Milwaukee, Educational Publications, American Vaccum Society, Wisconsin, pp. 23.
[40] W.R. Peifer, M.T. Coolbaugh, J.F. Garvey, J. Chem. Phys. 91 (1989) 6684.
[41] J.F. Garvey, R.B. Bernstein, Chem. Phys. Lett. 143 (1988) 13.
[42] T. Okabayashi, M. Tanimoto, J. Chem. Phys. 99 (1993) 3268.
[43] A.F. Wells (Ed.), Structural Organic Chemistry, 8th ed., 1991.
[44] V.Q. Nguyen, X.G. Chen, A.L. Yergey, J. Am. Soc. Mass Spectrom. 8 (1997) 1175.
[45] L. S. Farenzena, P. Iza, R. Martinez, F.A. Fernandez-Lima, E. D. Seperuelo, G.S. Faraudo, C.R. Ponciano, M.G.P. Homem, A. Naves de Brito, K. Wien, E.F. da Silveira, Earth, Moon, Planets, in press.
[46] T. Matsuo, T. Tonuma, H. Kumagai, H. Shibata, H. Tawara, J. Chem. Phys. 101 (1994) 5356.
[47] G.M. Lancaster, F. Honda, Y. Fukuda, J.W. Rabalais, J. Am. Chem. Soc. 101 (1979) 1951.
[48] S. Boudjadar, F. Haranger, T. Jalowy, A. Robin, B. Ban d'Etat, T. Been, Ph. Boduch, H. Lebius, B. Manil, L. Maunoury, H. Rothard, Eur. Phys. J. D32 (2005) 19.
[49] H.M. Urbassek, Nucl. Instrum. Meth. B 31 (1988) 541.
[50] A. Wucher, M. Wahl, Nucl. Instrum. Meth. B 115 (1996) 581.
[51] A.V. Hamza, T. Schenkel, A.V. Barnes, Eur. Phys. J. D6 (1999) 83.
[52] L.E. Rehn, R.C. Birtcher, S.E. Donnelly, P.M. Baldo, L. Funk, Phys. Rev. Lett. 87 (2001) 207601.
[53] C. Staudt, A. Wucher, Phys. Rev. B 66 (2002) 075419.